Exterior Shape Factors From Interior Shape Factors

Exterior Shape Factors From Interior Shape Factors

John H. Lienhard V
Rohsenow Kendall Heat Transfer Lab
Department of Mechanical Engineering,
Massachusetts Institute of Technology,
Cambridge, MA 02139-4307
e-mail: lienhard@mit.edu

Shape factors for steady heat conduction enable quick and highly simplified calculations of heat transfer rates within bodies having a combination of isothermal and adiabatic boundary conditions. Many shape factors have been tabulated, and most undergraduate heat transfer books cover their derivation and use. However, the analytical determination of shape factors for any but the simplest configurations can quickly come to involve complicated mathematics, and, for that reason, it is desirable to extend the available results as far as possible. In this paper, we show that known shape factors for the interior of two-dimensional objects are identical to the corresponding shape factors for the exterior of those objects. The canonical case of the interior and exterior of a disk is examined first. Then, conformal mapping is used to relate known configurations for squares and rectangles to the solutions for the disk. Both a geometrical and a mathematical argument are introduced to show that shape factors are invariant under conformal mapping. Finally, the general case is demonstrated using Green's functions. In addition, the "Yin-Yang" phenomenon for conduction shape factors is explained as a rotation of the unit disk prior to conformal mapping. [DOI: 10.1115/1.4042912]

Introduction

Shape factors for steady heat conduction have been tabulated in a number of publications [1,2], and most undergraduate heat transfer textbooks derive and use shape factors [3]. We consider two-dimensional (2D) objects (simple closed curves in the plane) that have portions of their boundary at either of two temperatures, with the sections between these adiabatic. The heat transfer rate $\dot{Q}$ (in W/m) across the interior of the body is

$$\dot{Q} = kS(T_1 - T_2) \tag{1}$$

where k is the thermal conductivity and S is the shape factor, which is dimensionless. For simple configurations, such as a rectangle or an annular sector with opposing isothermal edges, S is easily found; but for more complicated shapes, finding S rapidly becomes analytically difficult.

This difficulty is especially apparent when the aim is to find S for material *exterior* to a closed curve. For example, the solution for heat conduction from one side of the interior of a square of height a to the other side is trivial to find analytically: $\dot{Q} = ka\Delta T/a$, so $S = 1$. Yet, the solution for the exterior of the same case is very difficult to find analytically. A MATLAB solution based on high-resolution finite element calculations (Fig. 1) illustrates the nature of this complexity. However, we have made the empirical observation that, for some specific cases including this one, the exterior shape factor is the same as the interior shape factor.

This observation is unexpected because the heat transfer rates inside and outside need not be the same. The hot and cold boundaries act as a source and sink, respectively. Some amount of heat flows from the source to the interior and some amount flows, in the opposite direction, to the exterior. The thermal conductivities of the exterior and interior regions can be entirely different. Further, in general, the exterior heat flow would differ if other sources or sinks were present.

The primary aim of this work is to show that the interior and exterior shape factors are always equal under appropriate conditions. We have not seen this result in the literature on shape factors. We will show this result in several ways: for the fundamental case of a unit disk; as a property of conformal maps between arbitrary shapes and the unit disk (including a few examples of such maps); and for a more general region, by using Green's functions. We will assume that the only heat source and sink are the isothermal edges of the region, and we assume that the interior and exterior conductivities are uniform but not equal.

Formulation and Approach

For steady heat conduction in two dimensions, we are concerned with the Laplace equation for temperature, θ, scaled to $0 \leqslant \theta \leqslant 1$, with coordinates also nondimensionalized. For reasons discussed in the section Conformal Mapping and Shape Factors, it

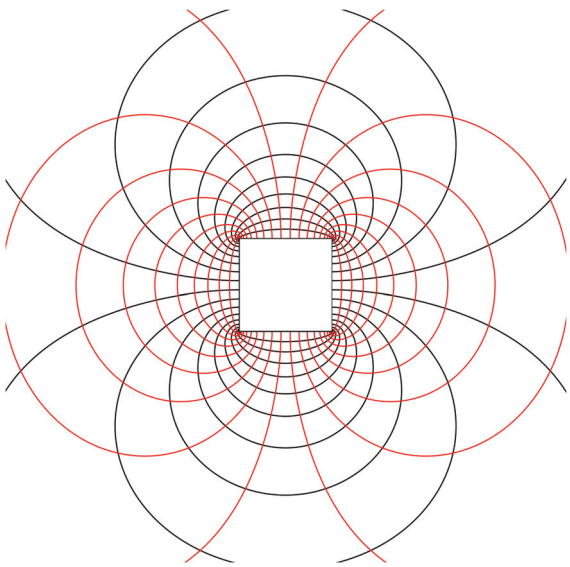

Fig. 1 Heat conduction outside a square. Vertical edges are isothermal at temperatures $\theta = 0$ and 1, and horizontal edges are adiabatic. (Numerical details in Appendix A). Twenty equally spaced isotherms are shown in red and twenty identically spaced adiabats in black, giving $n_i = 19$ temperature increments and $n_a = 19$ heat flow channels. Viewed as a flux plot [3], this figure shows that $S = n_a/n_i = 1$.

Contributed by the Heat Transfer Division of ASME for publication in the JOURNAL OF HEAT TRANSFER. Manuscript received September 3, 2018; final manuscript received January 12, 2019; published online April 16, 2019. Assoc. Editor: Yuwen Zhang.

is sufficient to consider the Dirichlet problem on the interior, R, of a simple closed curve, σ

$$\nabla^2\theta = 0 \quad \text{for } z \text{ in } R \tag{2}$$

$$\theta = h(z) \quad \text{for } z \text{ on } \sigma \tag{3}$$

where $z = (x, y)$ is the (possibly complex) coordinate in the plane and $h(z)$ is the distribution of temperature on the curve. The region R is simply connected. In some cases, we will consider the exterior Dirichlet problem for conduction in the region exterior to σ, in which case we consider the exterior region, E, to be the extended complex plane, including the point at infinity. For the exterior problem in two dimensions, in order for a steady-state solution to exist, there can be no heat transfer to the region far from the object. That condition is met if the temperature far from the object is the average temperature on any circle drawn around the outside of the object, by the mean value theorem for harmonic functions.[1] For objects having one high temperature side and one low temperature side, the far field will resemble that of a dipole.

The tools of conformal mapping are powerful and well developed for solution of the Laplace equation [4–7]. In particular, the *Riemann mapping theorem* guarantees that any simply connected region in the plane can be mapped to the unit disk. Solutions on the unit disk and the effect of mapping on shape factors are therefore of central importance to what follows. We will also be interested in rectangular regions that have simple conduction solutions, as a starting point for mapping shape factors to other geometries. We begin with heat conduction in the disk.

Temperature and Shape Factors Inside and Outside a Unit Disk. The Dirichlet problem for the *interior* of a unit disk $R = \{z : |z| < 1\}$ seeks the solution of Laplace's equation with a specified temperature distribution on the boundary $C = \{z : |z| = 1\}$. In polar coordinates, $r = |z|$ and $\phi = \arg z$, the boundary temperature can be written

$$\theta(1, \phi) = h(\phi) \tag{4}$$

The solution is provided by the Poisson integral formula [8]

$$\theta(r, \phi) = \int_{-\pi}^{\pi} P(r, \phi, \phi_0) h(\phi_0)\, d\phi_0 \tag{5}$$

with the Poisson kernel (Fig. 2)

$$P(r, \phi, \phi_0) = \frac{1}{2\pi} \frac{1 - r^2}{1 + r^2 - 2r\cos(\phi - \phi_0)} \tag{6}$$

The Poisson kernel represents the temperature at (r, ϕ) produced by a boundary temperature distribution that is a delta function at $(1, \phi_0)$; and Eq. (5) represents a superposition such temperature distributions along the boundary.

The exterior Dirichlet problem

$$\nabla^2\theta^e = 0, \quad r > 1 \tag{7}$$

$$\theta^e(1, \phi) = h(\phi) \tag{8}$$

is solved with a transformation that replaces r, for $r < 1$, in Eqs. (5) and (6) by $1/r$, for $r > 1$, with the result [5]

$$\theta^e(r, \phi) = -\int_{-\pi}^{\pi} P(r, \phi, \phi_0) h(\phi_0)\, d\phi_0 \tag{9}$$

Note that θ^e has a finite limit at infinity

[1]Compare to Eq. (10) and see discussion in the final section.

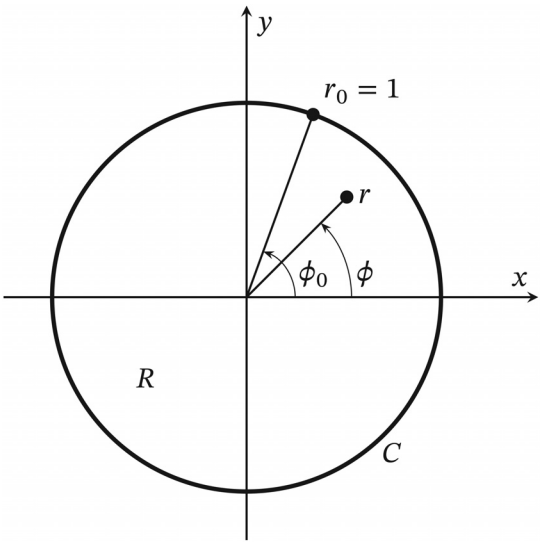

Fig. 2 Coordinates for the Poisson integral formula

$$\lim_{r\to\infty} \theta^e(r) = \frac{1}{2\pi}\int_{-\pi}^{\pi} h(\phi_0)\, d\phi_0 \tag{10}$$

In other words, the temperature at infinity is the average temperature around the perimeter of the unit disk. Because θ^e is bounded at infinity, the heat flux goes to zero as $1/r^2$ so that no heat is transferred to infinity.[2]

Interior and Exterior Shape Factors for a Disk are Equal. Consider a unit disk whose circular boundary C is a chain of four sections on which $h(\phi)$ takes different values

$$h(\phi) = \begin{cases} 0 & C_1 : -\pi < \phi < \phi_1 \\ h_{a,1}(\phi) & C_2 : \phi_1 \le \phi \le \phi_2 \\ 1 & C_3 : \phi_2 < \phi < \phi_3 \\ h_{a,2}(\phi) & C_4 : \phi_3 \le \phi \le \pi \end{cases} \tag{11}$$

In other words, section C_1 is isothermal at $\theta = 0$ and section C_3 is isothermal at $\theta = 1$. These two sections are joined by the temperature distributions $h_{a,1}(\phi)$ and $h_{a,2}(\phi)$, which vary smoothly from 0 to 1 and 1 to 0, respectively.

If the sections C_2 and C_4 were adiabatic, each would have some smoothly varying temperature distribution. Let us assume that these two distributions are none other than $h_{a,1}(\phi)$ and $h_{a,2}(\phi)$. We do not know the equations for these distributions; but, for the present purpose, it is sufficient that we know that they exist and correspond to the condition in which C_2 and C_4 are adiabatic. (An example of $h_{a,1}(\phi)$ is shown in Fig. 6.)

Considering first the interior Dirichlet problem, heat will flow from C_3 to C_1. No heat flows to C_2 or C_4, which are assumed adiabatic. Our normalization of temperature, T, to $0 \leqslant \theta \leqslant 1$ may be written $\theta = (T - T_1)/(T_3 - T_1)$, and radius is already nondimensionalized to $0 \leqslant r \leqslant 1$.

The interior shape factor can be found by evaluating the interior heat flow $\dot{Q}^i$ on just C_3. The heat flow is the integral over C_3 of the heat flux normal to the boundary. Heat flow going from C_3 to C_1 is taken to be positive, with $(T_3 - T_1)$ positive; under this convention, heat flux is opposite to the outward normal direction. Using the definition of the shape factor, Eq. (1), and the solution for θ, Eq. (5),

[2]The asymptotic expansion for $|z| \to \infty$ is $\theta^e(z) \sim \theta^e_\infty + a_1/z + a_2/z^2 + \cdots$ where θ^e_∞ is given by Eq. (10).

$$S^i = \frac{\dot{Q}^i}{k^i(T_3 - T_1)} = \int_{C_3} \frac{\partial\theta}{\partial n}\, dl = \int_{-\pi}^{\phi_1} \frac{\partial\theta}{\partial r}\bigg|_{r=1} d\phi \tag{12}$$

$$= \int_{-\pi}^{\phi_1} \frac{\partial}{\partial r} \int_{-\pi}^{\pi} P(r, \phi, \phi_0)\, h(\phi_0)\, d\phi_0 \bigg|_{r=1} d\phi \tag{13}$$

where k^i is the thermal conductivity inside the disk.

Note that the nondimensional heat flux at any angle ϕ on either C_2 or C_4 (presumed to be 0) is

$$-\frac{\partial\theta}{\partial r}\bigg|_{r=1} = -\frac{\partial}{\partial r} \int_{-\pi}^{\pi} P(r, \phi, \phi_0)\, h(\phi_0)\, d\phi_0 \bigg|_{r=1} = 0 \tag{14}$$

From Eq. (9), we can immediately see that the heat flux for the exterior solution must also be zero at every ϕ on these two boundaries

$$-\frac{\partial\theta^e}{\partial r}\bigg|_{r=1} = +\frac{\partial}{\partial r} \int_{-\pi}^{\pi} P(r, \phi, \phi_0)\, h(\phi_0)\, d\phi_0 \bigg|_{r=1} = 0 \tag{15}$$

If applied to C_1 or C_3, these results show that the heat flux of the interior solution at any ϕ is equal and opposite to the heat flux of the exterior solution at the same point.

The exterior shape factor may now be found, noting that θ^e has the finite limit as $r \to \infty$ that is required by Eq. (10). The exterior normal direction $\mathbf{n}^e$ is opposite to the interior normal direction $\mathbf{n}$. All heat transfer is from C_3 to C_1, with heat flowing away from C_3 into the exterior region and $(T_3 - T_1)$ positive. Using again the definition of S, with k^e the thermal conductivity outside the disk

$$S^e = \frac{\dot{Q}^e}{k^e(T_3 - T_1)} = \int_{C_3} \frac{\partial\theta^e}{\partial n^e}\, dl = -\int_{-\pi}^{\phi_1} \frac{\partial\theta^e}{\partial r}\bigg|_{r=1} d\phi \tag{16}$$

$$= \int_{-\pi}^{\phi_1} \frac{\partial}{\partial r} \int_{-\pi}^{\pi} P(r, \phi, \phi_0)\, h(\phi_0)\, d\phi_0 \bigg|_{r=1} d\phi \tag{17}$$

Comparing Eqs. (13) and (17), $S^i = S^e$. Note that the interior and exterior thermal conductivities need not be the same.

Conformal Mapping and Shape Factors

The Riemann mapping theorem shows that for a plane simply connected region R with boundary σ containing an interior point ζ, there exists a function $w = f(z, \zeta)$, analytic on R, that conformally maps R one-to-one onto the unit disk in the w-plane, taking σ to the disk's circumference and ζ to $w = 0$ [4,8]. When $\zeta = 0$, we will simply write $w = f(z)$. The mapping is unique to within an arbitrary rotation of the disk, and the significance of such rotations is discussed in the section Reverse Map From the Disk to the Square.

An important consequence of the Riemann mapping theorem is that if E is the portion of the extended complex plane[3] outside a simple closed curve σ, then E can be mapped conformally to the inside of the unit disk. For example, the bilinear transformation $(w = (az + b)/(cz + d))$ can take an exterior, unbounded region into a bounded region [7], and then the Riemann theorem guarantees a mapping onto the unit disk.

An elementary property of conformal maps is that isothermal boundaries map to isothermal boundaries and adiabatic boundaries map to adiabatic boundaries. Further, isotherms and adiabats remain orthogonal under conformal maps.

Shape Factors are Preserved Under Conformal Mapping. We now show that the shape factor of a region after mapping is the same as the shape factor for the region before mapping. The conformal invariance of electrical resistance is well known [9] and entirely analogous; but we have not seen the result in the heat transfer literature. We therefore provide the following simple (and perhaps original) explanation.

A conformal map preserves angles—which is why such mappings are useful in cartography—but the linear scale varies with position under mapping. In fact, a conformal mapping may be shown to consist of a rotation and a scalar multiplication of the original coordinates, where the angle of rotation and the scalar are different at different points. Call the scalar multiplier J. (Translation of the coordinates is also possible, but not important here.)

Consider an isothermal section of a boundary, which has a length Δl before mapping. If the temperature on this section is T and another isotherm a distance Δn away is at temperature $T + \Delta T$, then the heat flow through the section is

$$\Delta\dot{Q} = k\frac{\Delta T}{\Delta n}\Delta l \tag{18}$$

Now, suppose we map this region to another one. The mapped boundary section has length $J\ \Delta l$. The interior isotherm is at the same temperature as before mapping but now at a distance $J\ \Delta n$. Thus, the heat flow is

$$\Delta\dot{Q} = k\frac{\Delta T}{J\Delta n}(J\Delta l) = k\frac{\Delta T}{\Delta n}\Delta l \tag{19}$$

just as before the mapping. If we sum over all sections on each of the unmapped and mapped boundaries (i.e., integrate), we obtain the same total heat flow, $\dot{Q}$, for each.[4] In view of the definition, Eq. (1), S is the same before and after conformal mapping. (This result is demonstrated mathematically in Appendix B.)

Consider the conformal mapping of the interior of the unit disk to either the region R inside σ or the region E outside σ. For given boundary conditions, the interior shape factor of the disk is S. From the preceding argument, the shape factor for both R and E will have the same value of S under the mapped boundary conditions. Since the mappings are one-to-one, we can alternatively choose boundary conditions on R, map R to inside of the disk, and then map the disk to E, with the same S in all three cases.

The effect of the mappings on the boundary conditions requires additional consideration in each case. For example, the reciprocal map $(w = 1/z)$ takes the inside of the disk to the outside of the disk, but reflects the boundary conditions about the real axis. Additionally, the mappings to the disk are unique only to within an arbitrary rotation of the disk, so a rotational angle must be chosen to make the boundary conditions of a mapping to the inside correspond to those of the mapping to the outside. These issues are discussed in the examples that follow.

Proof of Principle: Examples on Squares and Disks

To demonstrate the ideas developed thus far, we will map reference cases for which the shape factor is known to cases for which it is not easily calculated. Two reference cases of interest are the interior of a square or a rectangle, for which the conduction problem is trivially solved. We map these onto the unit disk, which is less directly solvable. In particular, these cases illustrate: (i) the result of Eqs. (13) and (17), that shape factors interior and exterior to a disk are equal, (ii) the preservation of S under conformal mapping, (iii) the importance of rotations of the disk, and, (iv) the equality of the interior and exterior shape factors for the square.

Mapping a Square to the Unit Disk. Kober [6] provides a mapping of a square to the unit disk. Putting the square in the z-plane and the disk in the w-plane, the conformal map is

[3]The extended complex plane includes the point at infinity so that E is simply connected.

[4]The heat fluxes at any point are generally *not* the same.

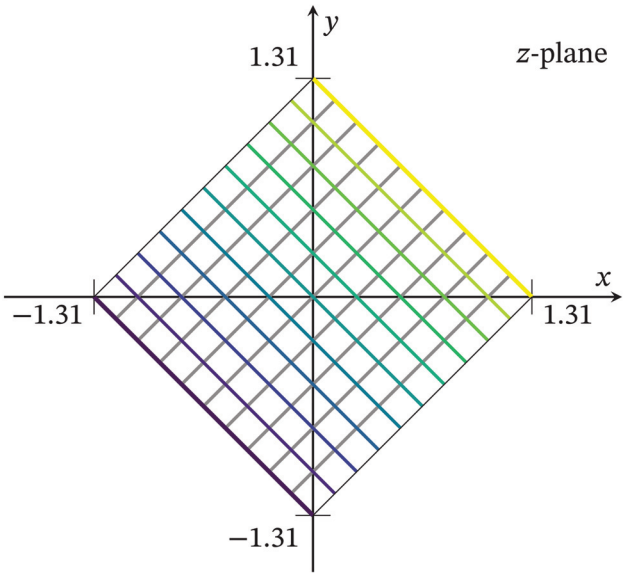

Fig. 3 Square with two isothermal sides and two adiabatic sides. Isotherms are in color and adiabats are in gray, $S = 1$.

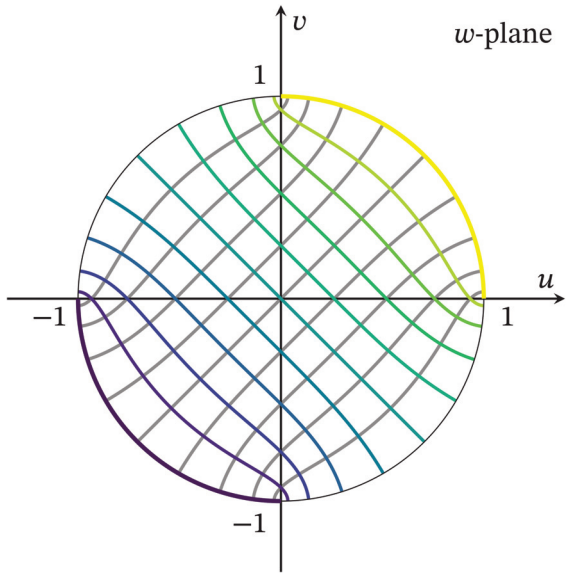

Fig. 4 Disk with two 90 deg isothermal edges and two opposing 90 deg adiabatic edges. Isotherms are in color and adiabats are in gray, $S = 1$.

$$w = f(z) = \sqrt{m}\,\frac{\mathrm{sn}\left(z/\sqrt{m}\,|\,m\right)}{\mathrm{dn}\left(z/\sqrt{m}\,|\,m\right)}, \quad \text{where } m = 1/2 \tag{20}$$

Here, $\mathrm{sn}(u\,|\,m)$ and $\mathrm{dn}(u\,|\,m)$ are complex-valued Jacobi elliptic functions of modulus m [10].[5] The corners of the square are normalized to be at $(w_1, 0)$, $(-w_1, 0)$, $(0, w_1)$, and $(0, -w_1)$, where

$$w_1 = \sqrt{m}\,\mathrm{arcsn}\left(1, \sqrt{m}\right) = \frac{1.85408\cdots}{\sqrt{2}} = 1.31103\cdots \tag{21}$$

The mapping takes the corner at $z = (w_1, 0)$ to $w = (1, 0)$, that at $z = (0, w_1)$ to $w = (0, 1)$, and so on. Variations on this mapping are discussed by Fong [11]. The inverse map, from w to z, is discussed below (see Eq. 30).

Eleven isotherms and eleven adiabats for the square are shown in Fig. 3. The solution for temperature, θ, is

$$\theta(x, y) = \frac{1}{2w_1}(x + y) + \frac{1}{2} \tag{22}$$

Parametric equations for the isotherms and adiabats as functions of x are useful for graphing the mapping. The lines are parametrized with the value of θ for each isotherm and a parameter n for each adiabat, with $0 \le n \le 1$:

$$y_{\mathrm{iso}} = (2\theta - 1)w_1 - x \quad \text{for isotherms} \tag{23}$$

$$y_{\mathrm{adi}} = x - (2n - 1)w_1 \quad \text{for adiabats} \tag{24}$$

The temperature along both adiabatic edges varies linearly from 0 to 1, and is given by

$$\theta = x/w_1 \quad \text{for the lower-right edge} \tag{25}$$

$$\theta = 1 + x/w_1 \quad \text{for the upper-left edge} \tag{26}$$

The shape factor for the square is $S = 1$ as previously discussed and as also evident because Fig. 3 has an equal number of heat flow channels and temperature increments: $n_a = n_i = 10$ so that $S = n_a/n_i = 1$.

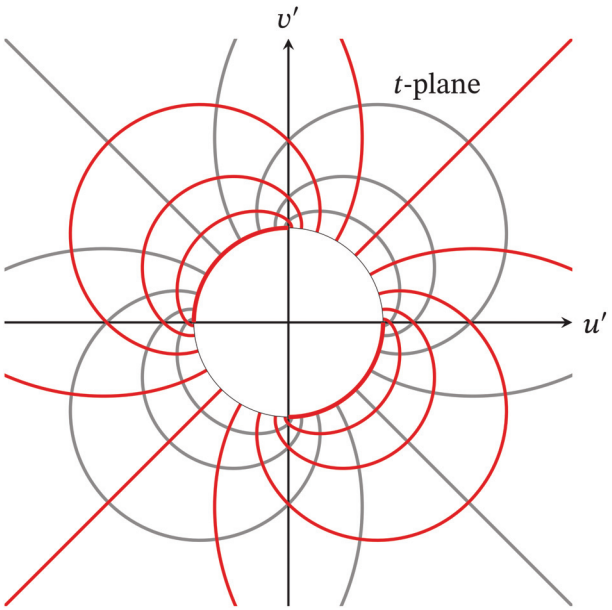

Fig. 5 Solution for heat conduction exterior to the 90 deg disk. Isotherms are in red and adiabats in gray. Note that the reciprocal map reflects the disk about the horizontal axis, $S = 1$.

The mapped disk is shown in Fig. 4.[6,7] This mapping produces a disk with opposing 90 deg isothermal edges and with the same number of temperature increments and heat flow channels as the original square: $S = 1$. The shape factor is obviously unchanged by any rotation of the disk as well.

The interior solution on the disk can be mapped to the exterior solution using the reciprocal map, which takes points (u, v) inside the disk in the w-plane to the outside of the disk in the t-plane: $t = 1/w$, with $t = (u', v')$. The result is shown in Fig. 5, where again there are ten heat flow channels and ten temperature increments. Consistent with the previous analysis, the shape factor for conduction on the exterior of the 90 deg disk is also $S = 1$. The reciprocal map reflects the boundary conditions about the x-axis, but this has no effect on S.

[5]Kober writes this expression in terms of the elliptic function parameter, k: $m = k^2$.

[6]The numerical methods are described in Appendix A.

[7]According to Ref. [9], this plot was first obtained by Schwarz in 1869.

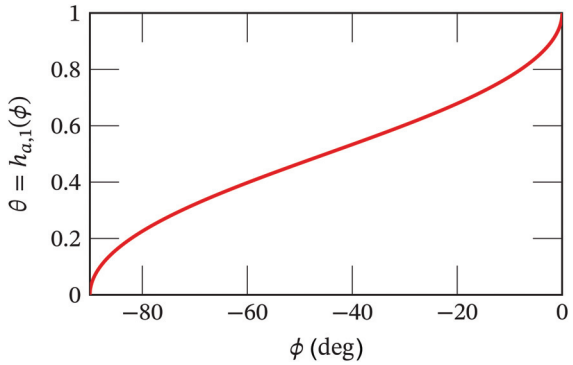

Fig. 6 Temperature distribution along one adiabatic edge of the disk

Finally, using the mapping function, we may plot the temperature distribution along either adiabatic edge (Fig. 6). This distribution is precisely the function $h_{a,1}(\phi)$ proposed in Eq. (11).

The solution for conduction exterior to the square is discussed later in this section.

Mapping a Rectangle to the Unit Disk. To show that $S^e = S^i$ for other boundary conditions on the disk, we may consider the conformal map that takes the interior of a rectangle whose vertices are $(\pm a, \pm b)$ onto the unit circle, $|w| \leq 1$ [12]:

$$w = f(z) = \frac{\mathrm{sn}(\lambda z \,|\, m)\,\mathrm{dn}(\lambda z \,|\, m)}{\mathrm{cn}(\lambda z \,|\, m)} \tag{27}$$

Here, $\mathrm{sn}(u \,|\, m)$, $\mathrm{cn}(u \,|\, m)$, and $\mathrm{dn}(u \,|\, m)$ are complex-valued Jacobi elliptic functions of modulus m, and

$$\lambda = \frac{K}{2a} = \frac{K'}{2b} \tag{28}$$

where $K(m)$ and $K'(m)$ are the real and imaginary quarter periods and m is calculated from this equation [12]. We may consider the edges at $\pm a$ to be isothermal and those at $\pm b$ to be adiabatic.

The result of this mapping is shown for three values of b/a in Figs. 7(*a*), 8(*a*), and 9(*a*). Because the shape factor for this rectangle is known to be

$$S_{\mathrm{rect}} = \frac{b}{a} \tag{29}$$

we have the corresponding shape factors on the unit disk with no further calculation. As before, the reciprocal map gives us the exterior conduction solution for each case (Figs. 7(*b*), 8(*b*), and 9(*b*)). And for each exterior case, the shape factor is again equal to that for the interior. Note also that Fig. 7(*a*), with $a = b$, is a square rotated by –45 deg relative to Fig. 4, a fact that will prove to be useful.

Reverse Map From Disk to Square and Yin-Yang Shape Factors. The conformal mapping from the square to the disk, Eq. (20), has the inverse function [6]

$$z = \int_0^w \frac{ds}{\sqrt{1 - s^4}} = \sqrt{2}\left[K(m) - F(\arccos w \,|\, m)\right] \tag{30}$$

where $K(m)$ is the complete Legendre elliptic integral of the first kind with modulus m and $F(\varphi \,|\, m)$ is the incomplete Legendre elliptic integral of the first kind with complex amplitude φ. The solution for the disk shown in Fig. 4 may be remapped to the z-plane using this inverse mapping, and the entirely unsurprising result is shown in Fig. 10(*a*).

A much more interesting result is obtained by mapping the *rotated* disk, Fig. 7(*a*), to the square because this mapping provides a solution for the square with isothermal half-boundaries at opposing corners (Fig. 10(*b*)). The solution interior (or exterior) to such a square is very difficult to calculate analytically; however, the conformal invariance of the shape factor dictates that $S = 1$ here as well. That $S = 1$ may be confirmed from Fig. 10(*b*), since the number of temperature increments equals the number of heat flow channels.

For other rotations of the disk prior to mapping to the square, the shape factor would be unchanged, but the boundary conditions on the square would rotate around the perimeter. Lengths are not preserved under conformal maps; however, the symmetries of disk and of the square require that half of the total boundary would remain adiabatic and half isothermal under rotation. Additionally, as a result of these symmetries: (i) if the boundary conditions are rotated about the origin by $\pi/2$, the isothermal and adiabatic boundaries of the square are interchanged; and (ii) if the rotation angle is π, the square's hot and cold boundaries are interchanged. None of these rotations affect S.

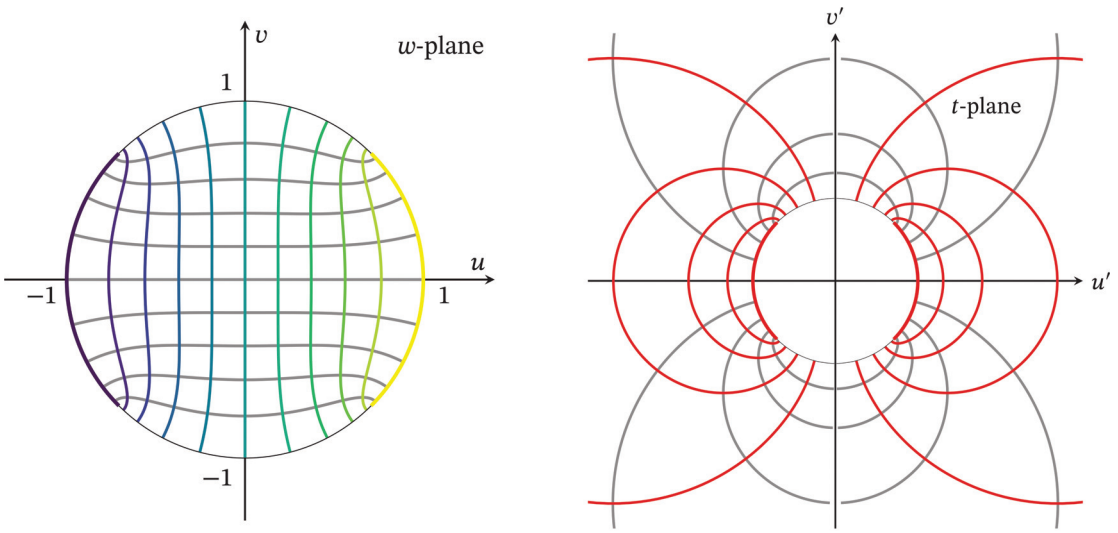

(*a*) (*b*)

Fig. 7 Mappings of a rectangle of aspect ratio $a:b = 1:1$ to the interior and exterior of a unit disk. The disk has two 90 deg isothermal edges and two opposing 90 deg adiabatic edges (boundary conditions rotated −45 deg from Fig. 4). Isotherms are in color and adiabats are in gray, $S = b/a = 1$: (*a*) map of a rectangle of 1:1 aspect ratio to interior of the unit disk and (*b*) map of a rectangle of 1:1 aspect ratio to exterior of the unit disk.

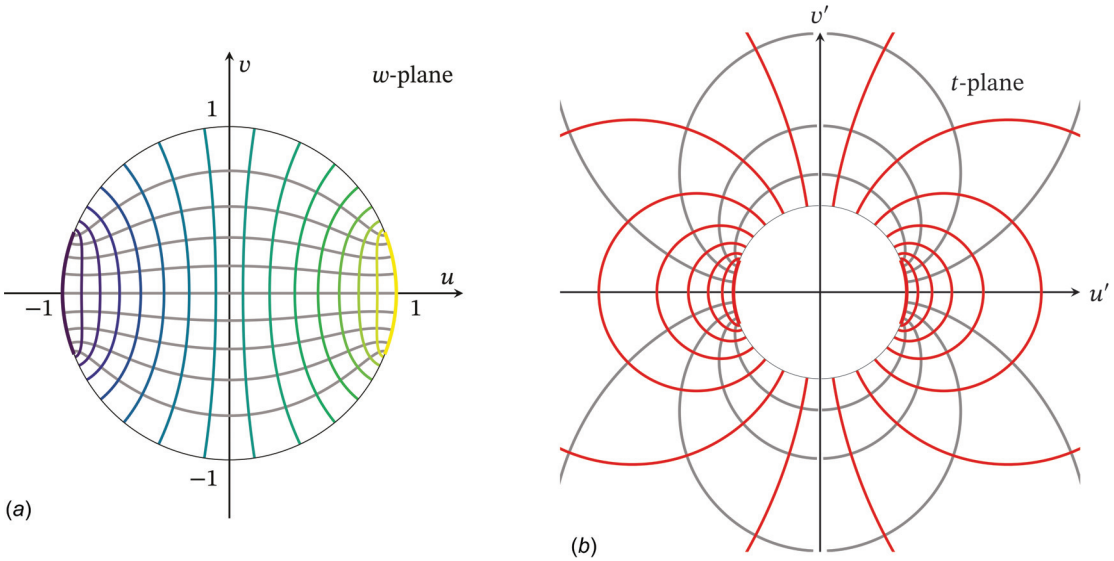

Fig. 8 Mappings of a rectangle of aspect ratio $a:b = 1.5:1$ to the interior and exterior of a unit disk, $S = b/a = 2/3$. Sixteen isotherms are in color and eleven adiabats are in gray: (*a*) map of a rectangle of 1.5:1 aspect ratio to interior of the unit disk and (*b*) map of a rectangle of 1.5:1 aspect ratio to exterior of the unit disk.

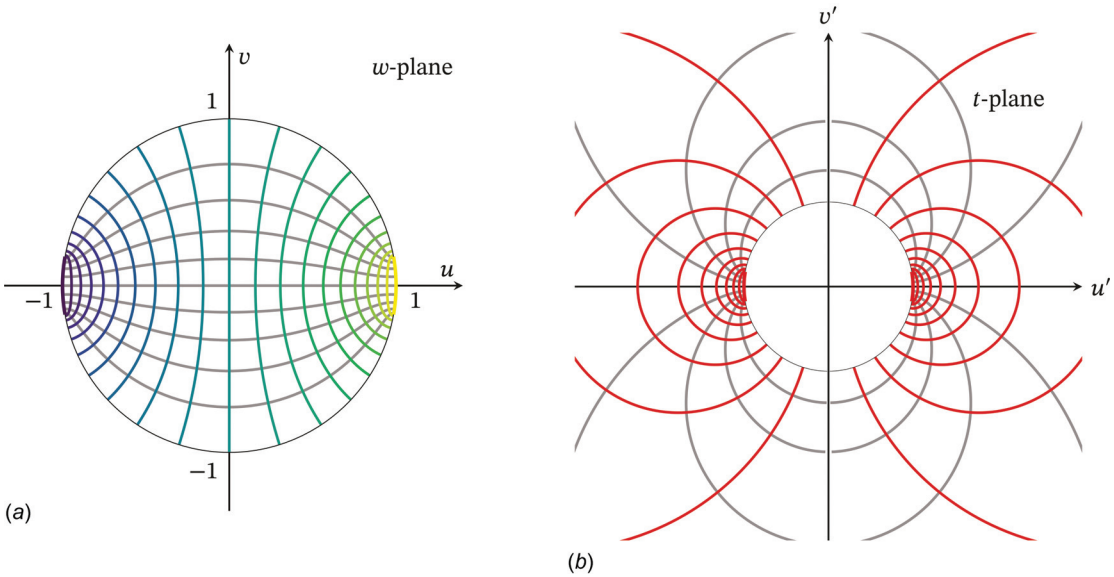

Fig. 9 Mappings of a rectangle of aspect ratio $a:b = 2:1$ to the interior and exterior of a unit disk. Isotherms are in color and adiabats are in gray, $S = b/a = 1/2$: (*a*) map of a rectangle of 2:1 aspect ratio to interior of the unit disk and (*b*) map of a rectangle of 2:1 aspect ratio to exterior of the unit disk.

In fact, these rotated cases are examples of a larger class of so-called Yin-Yang bodies described by Lienhard [13] for which $S = 1$. The Yin-Yang bodies are those having a geometrical axis of symmetry on either side of which the adiabatic and isothermal boundary conditions are interchanged. In Fig. 10(*a*), this axis of symmetry is either the x- or the y-axis; in Fig. 10(*b*), the axis of symmetry is a line through the origin at either 45 deg or –45 deg; and in Fig. 4, the axis of symmetry is either the u- or the v-axis. (In fact, the situations in Fig. 10 are examples 2a and 2b from Ref. [13].) In contrast, Figs. 8(*a*) and 9(*a*) lack this symmetry. We may now state that *all* Yin-Yang configurations should be reducible to conformal mappings from the unit disk, with the boundary conditions of Fig. 7(*a*), under differing rotations of the disk about the origin.

The mapping from the interior of the disk to the exterior of the square is

$$z = \int_{w_0}^{w} \frac{\sqrt{1 - s^4}}{s^2}\, ds \tag{31}$$

where $|w| \leq 1$ [4]. The integral does not converge as $|w_0| \to 0$, since that is the point at infinity in the z-plane. We have already presented a finite element solution for the exterior in Fig. 1, showing that $S = 1$, so we will not compute this mapping.

Green's Functions for an Arbitrary Two-Dimensional Region, *R*

We now generalize the analysis done for the unit disk to any arbitrary two-dimensional region R with a simple closed boundary σ that may have any shape (Fig. 11(*a*)). The vector $\mathbf{n}$ is the unit outward normal to σ. The Green's function $g(z|\zeta)$ is the solution of the following equation:

$$-\nabla^2 g = \delta(\zeta - z) \tag{32a}$$

$$z \text{ and } \zeta \text{ in } R \tag{32b}$$

$$g = 0 \text{ for } \zeta \text{ on } \sigma \tag{32c}$$

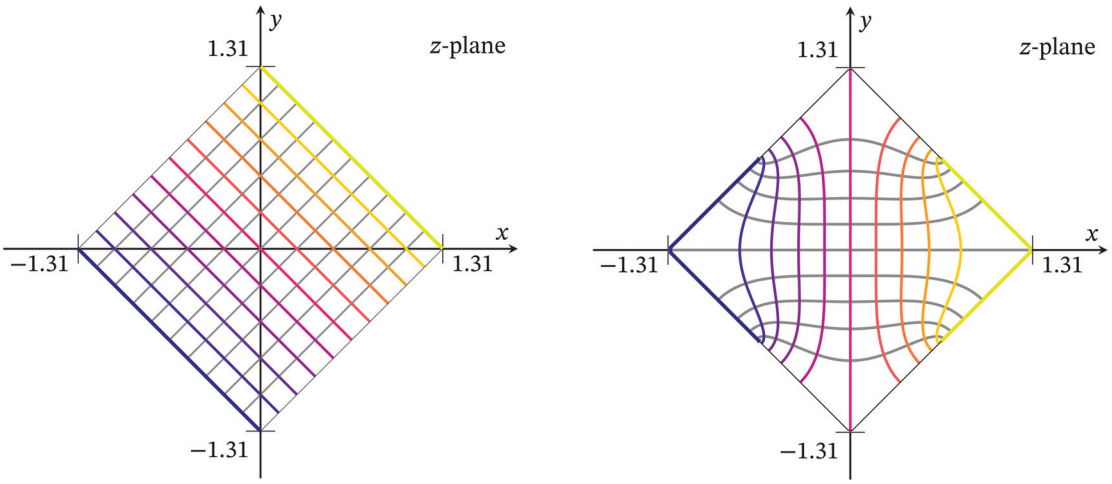

Fig. 10 Solutions for heat conduction interior to the square obtained using the reverse mapping by Eq. (30) from the disk for two sets of boundary conditions. Both are Yin-Yang configurations [13]: (*a*) the reverse mapping from the disk to the square, $S=1$, and (*b*) rotated boundary conditions based on the rectangle with $a/b=1$, $S=1$.

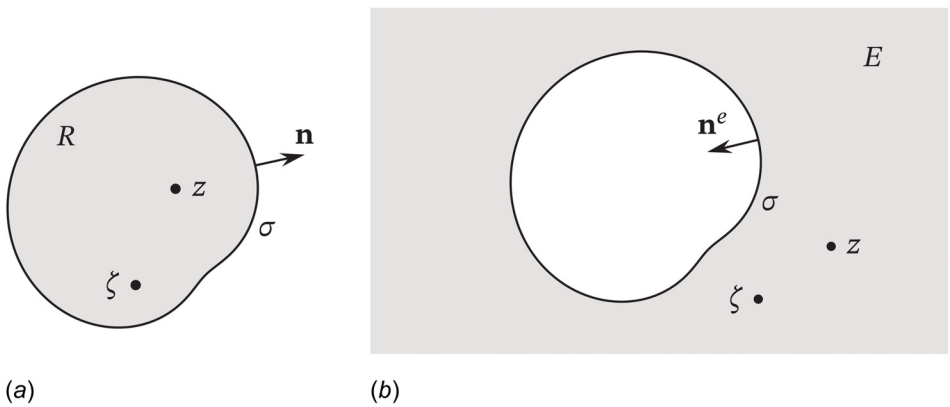

Fig. 11 Configuration and coordinates for Green's functions: (*a*) interior region and (*b*) exterior region

We may find the solution of the Dirichlet problem, Eqs. (2) and (3), using Green's second identity. We treat g and θ as functions of ζ [8]

$$\int_R \left[g\nabla^2\theta - \theta\nabla^2 g\right] dR_\zeta = \int_\sigma \left[g\frac{\partial\theta}{\partial n_\zeta} - \theta\frac{\partial g}{\partial n_\zeta}\right] dl_\zeta \tag{33}$$

where the subscript ζ indicates that differentiation or integration is with respect to the ζ coordinate. Substituting from Eqs. (3) and (32) leads to an expression for θ as an integral around the boundary

$$\theta(z) = -\int_\sigma \frac{\partial g(z|\zeta)}{\partial n_\zeta} h(\zeta)\, dl_\zeta \equiv \int_\sigma I(z|\zeta)\, h(\zeta)\, dl_\zeta \tag{34}$$

The boundary influence function $I(z|\zeta)$ is defined as shown. This result is like Eq. (5). The influence function is the temperature at z that would be produced by a boundary temperature that is a delta function at ζ (e.g., like a unit-strength point source). The integral is a superposition of such sources of strength $h(\zeta)$ around the boundary σ.

For the region exterior to σ, E, the formulation is the same, with the exception that the outward normal direction, $\mathbf{n}^e$, is opposite $\mathbf{n}$ (Fig. 11(*b*))

$$\theta^e(z) = -\int_\sigma \frac{\partial g^e(z|\zeta)}{\partial n^e_\zeta} h(\zeta)\, dl_\zeta = \int_\sigma \frac{\partial g^e(z|\zeta)}{\partial n_\zeta} h(\zeta)\, dl_\zeta \tag{35}$$

We also require $g^e(z, \zeta)$ to produce a bounded solution for θ^e as $|z| \to \infty$ [8].

Since there are no temperature sources other than the boundary σ, we may also write the exterior solution directly in terms of the boundary influence function, respecting the change in normal direction

$$\theta^e(z) = -\int_\sigma I(z|\zeta)\, h(\zeta)\, dl_\zeta \tag{36}$$

The Green's function for R may be written in terms of the conformal map f that takes $z \in R$ to the unit disk and the point $\zeta \in R$ to $w=0$ [4,8]

$$g(z|\zeta) = -\frac{1}{2\pi}\log|f(z,\zeta)| \tag{37}$$

Green's Functions for the Unit Disk. As a specific example, when R is unit disk (Fig. 12), the bilinear mapping from the disk to itself is

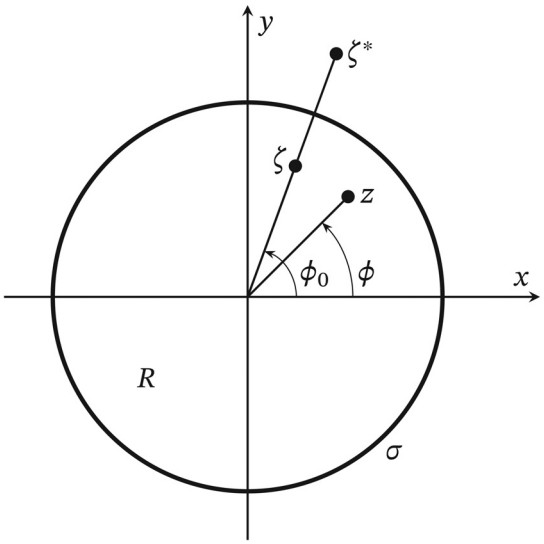

Fig. 12 Coordinates for the Green's function on the unit disk

$$w = f(z,\zeta) = \frac{z-\zeta}{1-z\bar{\zeta}} \tag{38}$$

where $\bar{\zeta}$ is the complex conjugate of ζ, and so the interior Green's function is

$$\begin{aligned} 2\pi\, g(z|\zeta) &= -\log\left|\frac{z-\zeta}{1-z\bar{\zeta}}\right| \\ &= -\log|z-\zeta| + \log|z-\zeta^*| + \log|\zeta| \end{aligned} \tag{39}$$

where $\zeta^* = (1/|\zeta|)\, e^{i\phi_0}$ is the image of ζ with respect to the circle (cf. Ref. [8]). In polar coordinates, $z=(r,\ \phi)$ and $\zeta=(r_0,\ \phi_0)$. Then, with reference to Fig. 12, the law of cosines gives

$$|z-\zeta|^2 = r_0^2 - 2rr_0\cos(\phi-\phi_0) + r^2 \tag{40}$$

In particular, if ζ is on the unit circle, $r_0=1$ and

$$|z-\zeta|^2 = 1 - 2r\cos(\phi-\phi_0) + r^2 \tag{41}$$

With this information, a lengthy but straightforward calculation shows that the influence function, $I(z|\zeta)$, for the disk is simply the Poisson kernel, Eq. (6)

$$I(z|\zeta) = -\left.\frac{\partial g(z|\zeta)}{\partial n_\zeta}\right|_\sigma = -\left.\frac{\partial g(z|\zeta)}{\partial r_0}\right|_{r_0=1} = \cdots = P(r,\phi,\phi_0) \tag{42}$$

The right-hand side of Eq. (39) consists of sources at ζ and at its image point ζ*, plus a constant term that makes $g=0$ for z on σ. If z and ζ lie outside the unit disk, the Green's function is unaffected; and so Eq. (39) is also $g^e(z|\zeta)$.[8] The normal direction, however, is reversed for the exterior problem. Thus, with Eq. (35), we see that the exterior solution is just Eq. (36) and that the result is consistent with Eq. (9). Note that $g^e(z|\zeta)\to 0$ as $|z|\to\infty$.

Interior and Exterior Shape Factors of *R* are Equal. As for the unit disk, we can imagine the boundary of R, σ, to be composed of a chain four curves, σ_1 isothermal at $\theta=0$, σ_2 and σ_4 adiabatic, and σ_3 isothermal at $\theta=1$. The boundary need not be circular. The shape factor for the interior problem is

$$S^i = \int_{\sigma_3}\frac{\partial\theta}{\partial n_z}\,dl_z = -\int_{\sigma_3}\frac{\partial}{\partial n_z}\int_\sigma \frac{\partial g(z|\zeta)}{\partial n_\zeta}\,h(\zeta)\,dl_\zeta dl_z \tag{43}$$

$$= +\int_{\sigma_3}\frac{\partial}{\partial n_z}\int_\sigma I(z|\zeta)\,h(\zeta)\,dl_\zeta dl_z \tag{44}$$

For the exterior problem, the normal direction is reversed

$$S^e = \int_{\sigma_3}\frac{\partial\theta^e}{\partial n_z^e}\,dl_z = -\int_{\sigma_3}\frac{\partial}{\partial n_z^e}\int_\sigma \frac{\partial g^e(z|\zeta)}{\partial n_\zeta^e}\,h(\zeta)\,dl_\zeta dl_z \tag{45}$$

$$= -\int_{\sigma_3}\frac{\partial}{\partial n_z}\int_\sigma \frac{\partial g^e(z|\zeta)}{\partial n_\zeta}\,h(\zeta)\,dl_\zeta dl_z \tag{46}$$

$$= +\int_{\sigma_3}\frac{\partial}{\partial n_z}\int_\sigma I(z|\zeta)\,h(\zeta)\,dl_\zeta dl_z \tag{47}$$

where in the second step, we revert to the interior normal direction, with signs canceling; and in the third step, we substitute from Eqs. (35) and (36). Comparing Eq. (44) to Eq. (47), we see again that $S^e = S^i$.

Boundary Condition as $|\mathbf{z}|\to\infty$. In order for solutions to these two-dimensional problems to exist, the temperature at infinity must be bounded[9] and take on a specific value that ensures no net heat transfer to locations distant from the boundary, σ.

For the circular disk, Eq. (10) provides the necessary temperature at large radius. For boundary conditions that have appropriate reflectional symmetry, this temperature is easily seen to be $\theta=1/2$, as for the situations in Figs. 5, 7(*b*), 8(*b*), and 9(*b*). However, for asymmetric conditions, the far-field temperature may take some other value between 0 and 1. For example, a disk with 357 deg of its boundary at $\theta=1$, two adiabatic segments of 1 deg arc, and a 1 deg segment at $\theta=0$ would require a far field temperature only slightly below 1, roughly $\theta\approx 358/360$.

For noncircular boundaries, symmetrical cases like Fig. 1 may also have a far field temperature of $\theta=1/2$. In other instances, the mean value theorem for harmonic functions can be applied in the form of Eq. (10). Specifically, for any circle in E that encompasses σ, the integral of temperature around the circle gives the limiting value of temperature as $|z|\to\infty$. By constructing such a circle for a given object, the necessary condition at infinity may be estimated or calculated.

Conclusions

We have considered conduction shape factors for two-dimensional, simply connected objects that have two isothermal boundaries, each at different temperature and separated by two adiabatic boundaries. The primary result obtained is:

- *Shape factors for conduction inside an object are equal to those for conduction through the material outside the object*, if the only heat sources and sinks are the isothermal segments of the boundary and there is no net heat transfer to the exterior region at great distance from the object. The interior and exterior thermal conductivities must be uniform, but need not be equal.

In addition,

- Both geometrical and mathematical proofs are given to show that conduction shape factors are invariant when an object is conformally mapped onto another object. While this principle is known in other contexts (e.g., for electrical resistance),

[8]In fact, Eq. (38) also maps the region exterior to the unit disk into the unit disk, so this result is expected from Eq. (37).

[9]The exterior Dirichlet problem can include terms that logarithmically diverge at large distances, so the coefficients of such terms must be zero.

the present original arguments may be useful for instructional purposes.
- The Yin-Yang shape factors with $S = 1$, first described in 1981, have been explained as rotations of the unit disk, Fig. 7(*a*), prior to conformal mapping.

Acknowledgment

The observation that interior and exterior shape factors are equal arose during a conversation with John H. Lienhard (IV). The MATLAB code used to produce Fig. 1 was based in part on a code provided by Andrew J. Lienhard. Both have made a number of helpful comments on the manuscript.

Nomenclature

a, b = dimensionless length of sides of square or rectangle
C = circular curve
E = simply connected region exterior to curve
$f(z,\zeta), f(z)$ = conformal mapping function
$g(z|\zeta)$ = Green's function
$h(z)$, $h(\phi)$ = temperature distribution on boundary
$h_a(\phi)$ = temperature distribution on adiabatic edge, Eq. (11)
$I(z|\zeta)$ = influence function, Eq. (34)
J = scalar multiplier
$\boldsymbol{J}_1, \boldsymbol{J}_2$ = Jacobian matrices
k = thermal conductivity (W m^{-1} K^{-1})
l = position along a curve
m = modulus of elliptic function
n_a = number of heat flow channels
n_i = number of temperature increments
$\mathbf{n}$ = unit normal vector
$P(r, \phi, \phi_0)$ = Poisson kernel, Eq. (6)
$\dot{Q}$ = heat transfer rate (W m^{-1})
r = polar radius, $|z|$
r_0 = polar radius, $|\zeta|$
R = simply connected region interior to curve
S = shape factor, Eq. (1)
T = temperature (K)
(u, v) = real, imaginary coordinates in the w-plane
(u', v') = real, imaginary coordinates in the t-plane
$w, \mathbf{w}$ = position in the complex w-plane
w_1 = constant given by Eq. (21)
(x, y) = real, imaginary coordinates in the z-plane
$z, \mathbf{z}$ = position in the complex z-plane

Greek and Other Symbols

α, β = see Eq. (B4)
$\delta(z)$ = Dirac delta function
Δ = difference in a quantity
ζ = source position in the complex plane
ζ^* = image of ζ with respect to circle
θ = dimensionless temperature
λ = constant defined by Eq. (28)
σ = simple closed curve
φ = complex amplitude of elliptic integral
ϕ = polar angle, arg z
ϕ_0 = polar angle, arg ζ and arg ζ^*
$\nabla^\perp$ = skew gradient, Eq. (B2)

Superscripts and Subscripts

e = exterior value
i = interior value
T = transpose of matrix or vector
w = evaluated with respect to w
z = evaluated with respect to z
ζ = evaluated with respect to ζ
$\bar{}$ = complex conjugate

Appendix A: Numerical Implementation

Figure 1 was generated using MATLAB's finite element method algorithms with 181,700 nodes to compute both harmonic conjugates, which were then interpolated to a 501×501 grid and overlaid. The computational domain had 100 times the area of the inner square and had a square external boundary at the average perimeter temperature of the interior square ($\theta = 1/2$). Only the inner 30% of the computational domain is shown in the figure; however, temperature variation in the excluded region is less than 10% of the overall temperature difference.

The other charts were computed using Lua code [14] under LuaLaTeX [15] using TEXShop and TEX Live [16]. The resulting Lua functions were supplied to PGFPLOTS [17] to generate the charts. The elliptic integrals were executed using the GNU SCIENTIFIC LIBRARY [18] with FFI bindings to Lua [19], following the complex amplitude formulæ in Ref. [10]. The GSL C code was compiled using XCode under Mac OS X. The elliptic functions were computed in Lua using an algorithm from Press et al. [20], again applying complex argument formulæ from Ref. [10].

Several of the figures use the perceptually uniform colormaps, Viridis and Plasma, by van der Walt and Smith [21].

Appendix B: Line Integral of a Normal Derivative

We can more formally demonstrate that the integral defining the shape factor is unchanged by a conformal map. Consider an integral in the mapped w-plane, and for convenience write this in vector notation

$$\int_\sigma \frac{\partial T}{\partial n}\, dl = \int_\sigma \mathbf{n} \cdot \nabla T\, dl = \int_\sigma \nabla^\perp T \cdot d\mathbf{w} \tag{B1}$$

in which the skew gradient is

$$\nabla^\perp T \equiv \begin{pmatrix} \partial T/\partial v \\ -\partial T/\partial u \end{pmatrix} \tag{B2}$$

The transformation of $d\mathbf{w}$ to the z-plane is

$$d\mathbf{w} = \begin{pmatrix} du \\ dv \end{pmatrix} = \underbrace{\begin{pmatrix} \partial u/\partial x & \partial u/\partial y \\ \partial v/\partial x & \partial v/\partial y \end{pmatrix}}_{=\boldsymbol{J}_1} \begin{pmatrix} dx \\ dy \end{pmatrix} \tag{B3}$$

Using the Cauchy–Riemann conditions, $\partial u/\partial x = \partial v/\partial y$ and $\partial u/\partial y = -\partial v/\partial x$, the determinant is $|\boldsymbol{J}_1| = (\partial u/\partial x)^2 + (\partial u/\partial y)^2$ and so

$$\boldsymbol{J}_1 = |\boldsymbol{J}_1| \begin{pmatrix} \alpha & \beta \\ -\beta & \alpha \end{pmatrix} \tag{B4}$$

where $\alpha^2 + \beta^2 = 1$. The matrix in this equation is a rotation, and $|\boldsymbol{J}_1|$ reports the change in u that results from a change in z

$$\left|\frac{\partial u}{\partial z}\right|^2 = \frac{\partial u}{\partial z}\frac{\overline{\partial u}}{\partial z} = \left(\frac{\partial u}{\partial x}\right)^2 + \left(\frac{\partial u}{\partial y}\right)^2 \tag{B5}$$

Similarly, the transformation of the skew gradient is

$$\nabla^\perp T = \begin{pmatrix} \partial T/\partial v \\ -\partial T/\partial u \end{pmatrix} = \underbrace{\begin{pmatrix} \partial y/\partial v & -\partial x/\partial v \\ -\partial y/\partial u & \partial x/\partial u \end{pmatrix}}_{=\boldsymbol{J}_2} \begin{pmatrix} \partial T/\partial y \\ -\partial T/\partial x \end{pmatrix} \tag{B6}$$

$$= |\boldsymbol{J}_2| \begin{pmatrix} \alpha & \beta \\ -\beta & \alpha \end{pmatrix} \begin{pmatrix} \partial T/\partial y \\ -\partial T/\partial x \end{pmatrix} \tag{B7}$$

where $|\boldsymbol{J}_2| = (\partial x/\partial u)^2 + (\partial y/\partial u)^2$. $|\boldsymbol{J}_2|$ reports the change in z that results from a change in u

$$\left|\frac{\partial z}{\partial u}\right|^2 = \frac{\partial z}{\partial u}\frac{\partial \bar{z}}{\partial u} = \left(\frac{\partial x}{\partial u}\right)^2 + \left(\frac{\partial y}{\partial u}\right)^2 \tag{B8}$$

Thus, $|\boldsymbol{J}_1|\,|\boldsymbol{J}_2| = |\partial u/\partial z|^2 |\partial z/\partial u|^2 = 1$, and α and β have the same values in Eqs. (B4) and (B7).

To evaluate the inner product $(\nabla^{\perp} T)\cdot(d\mathbf{w})$, we may use the transpose properties of matrix products. For vectors $\mathbf{a}$ and $\mathbf{b}$ and matrices $\boldsymbol{A}$ and $\boldsymbol{B}$

$$(\boldsymbol{A}\mathbf{a})\cdot(\boldsymbol{B}\mathbf{b}) = (\boldsymbol{A}\mathbf{a})^{\mathrm{T}}(\boldsymbol{B}\mathbf{b}) = \mathbf{a}^{\mathrm{T}}\boldsymbol{A}^{\mathrm{T}}(\boldsymbol{B}\mathbf{b}) = \mathbf{a}^{\mathrm{T}}(\boldsymbol{A}^{\mathrm{T}}\boldsymbol{B})\mathbf{b} \tag{B9}$$

Then, using Eqs. (B3) and (B6)

$$\nabla^{\perp} T \cdot d\mathbf{w} = \begin{pmatrix} \partial T/\partial y \\ -\partial T/\partial x \end{pmatrix}^{\mathrm{T}} \boldsymbol{J}_2^{\mathrm{T}} \boldsymbol{J}_1 \begin{pmatrix} dx \\ dy \end{pmatrix} \tag{B10}$$

Multiplication of the Jacobian matrices produces a considerable simplification

$$\boldsymbol{J}_2^{\mathrm{T}} \boldsymbol{J}_1 = |\boldsymbol{J}_2|\,|\boldsymbol{J}_1| \begin{pmatrix} \alpha & -\beta \\ \beta & \alpha \end{pmatrix} \begin{pmatrix} \alpha & \beta \\ -\beta & \alpha \end{pmatrix} \tag{B11}$$

$$= |\boldsymbol{J}_1|\,|\boldsymbol{J}_2| \begin{pmatrix} \alpha^2+\beta^2 & 0 \\ 0 & \alpha^2+\beta^2 \end{pmatrix} \tag{B12}$$

$$= |\boldsymbol{J}_1|\,|\boldsymbol{J}_2| \begin{pmatrix} 1 & 0 \\ 0 & 1 \end{pmatrix} \tag{B13}$$

$$= \begin{pmatrix} 1 & 0 \\ 0 & 1 \end{pmatrix} \tag{B14}$$

Putting these pieces together, denoting the w and z planes by subscripts, we find that

$$\int_{\sigma_w} \mathbf{n}\cdot\nabla_w T\, dl_w = \int_{\sigma_w} \nabla_w^{\perp} T \cdot d\mathbf{w} = \int_{\sigma_z} \nabla_z^{\perp} T \cdot d\mathbf{z} = \int_{\sigma_z} \mathbf{n}\cdot\nabla_z T\, dl_z \tag{B15}$$

In words, line integrals of the normal derivative are unchanged by conformal maps.

References

[1] Hahne, E., and Grigull, U., 1975, "Formfactor and Formwiderstand Der Stationären Mehrdimensionalen Wärmeleitung," Int. J. Heat Mass Transfer, **18**(6), pp. 751–767.

[2] Yovanovich, M. M., 1998, "Conduction and Thermal Contact Resistances (Conductances)," *Handbook of Heat Transfer*, 3rd ed., W. M. Rohsenow, J. P. Hartnett, and Y. I. Cho, eds., McGraw-Hill, New York, Chap. 3.

[3] Lienhard, J. H., IV, and Lienhard, J. H., V, 2018, *A Heat Transfer Textbook*, 4th ed., Phlogiston Press, Cambridge, MA.

[4] Nehari, Z., 1952, *Conformal Mapping*, McGraw-Hill Book Company, New York.

[5] Brown, J. W., and Churchill, R. V., 2009, *Complex Variables and Applications*, 8th ed., McGraw-Hill, New York.

[6] Kober, H., 1957, *Dictionary of Conformal Representations*, Dover Publications, Mineola, NY.

[7] Weinberger, H. F., 1965, *A First Course in Partial Differential Equations*, Blaisdell Publishing Company, New York.

[8] Stakgold, I., 1967, *Boundary Value Problems of Mathematical Physics*, Macmillan, New York.

[9] Driscoll, T. A., and Trefethen, L. N., 2002, *Schwarz-Christoffel Mapping*, Cambridge University Press, Cambridge, UK.

[10] Abramowitz, M., and Stegun, I. A., 1964, *Handbook of Mathematical Functions*, U.S. National Bureau of Standards, Washington, DC.

[11] Fong, C., 2015, "Analytical Methods for Squaring the Disc," e-print https://arxiv.org/abs/1509.06344v3

[12] Milne-Thomson, L. M., 1950, *Jacobian Elliptic Function Tables*, Dover Publications, New York.

[13] Lienhard, J. H., 1981, "Heat Conduction Through 'Yin-Yang' Bodies," ASME J. Heat Transfer, **103**(3), pp. 600–601.

[14] lerusalimschy, R., de Figueiredo, L. H., and Celes, W., 2017, *Lua 5.3 Reference Manual*, Pontifical Catholic University, Rio de Janeiro, Brazil, accessed Mar. 7, 2019, https://www.lua.org/manual/5.3/

[15] Montijano, J. I., Pérez, M., Rández, L., and Varona, J. L., 2014, "Numerical Methods With LuaLaTeX," TUGboat, **35**(1), pp. 51–56.

[16] Koch, R., 2018, "TEXShop," University of Oregon, Eugene, OR, Version 4.01, accessed Mar. 7, 2019, http://pages.uoregon.edu/koch/texshop/obtaining.html

[17] Feuersänger, C., 2017, *Manual for Package PGFPLOTS, Version 1.15*, SourceForge Media, La Jolla, CA, accessed Mar. 7, 2019, http://sourceforge.net/projects/pgfplots

[18] Galassi, M., Davies, J., Theiler, J., Gough, B., Jungman, G., Alken, P., Booth, M., Rossi, F., and Ulerich, R., 2017, *GNU Scientific Library Release 2.4*, Free Software Foundation, Boston, MA, accessed Mar. 7, 2019, https://www.gnu.org/software/gsl/

[19] Menke, H., 2018, "Tutorial: Using External C Libraries With the LuaLaTeX FFI," TUGboat, **39**(1), pp. 37–40.

[20] Press, W. H., Teukolsky, S. A., Vetterling, W. T., and Flannery, B. P., 1986, *Numerical Recipes*, Cambridge University Press, Cambridge, UK.

[21] van der Walt, S., and Smith, N., 2015, "*mpl Colormaps*," GitHub, San Francisco, CA, accessed Aug. 26, 2018, http://bids.github.io/colormap/